Mathematical Biosciences and Engineering

MBE, 20(8): 14811–14826.
DOI: 10.3934/mbe.2023663
Received: 01 May 2023
Revised: 15 June 2023
Accepted: 24 June 2023
Published: 10 July 2023

http://www.aimspress.com/journal/MBE

*Research article*

# Comparison of homemade mask designs based on calculated infection risk, using actual COVID-19 infection scenarios

**Shayna Berman, Gavin D'Souza, Jenna Osborn and Matthew Myers***

Division of Applied Mechanics, U. S. FDA/CDRH, 10903 New Hampshire Avenue, Silver Spring 20993, MD, USA

* **Correspondence:** Email: Matthew.myers@fda.hhs.gov; Tel: 3017962525.

**Abstract:** During pandemics such as COVID-19, shortages of approved respirators necessitate the use of alternative masks, including homemade designs. The effectiveness of the masks is often quantified in terms of the ability to filter particles. However, to formulate public policy the efficacy of the mask in reducing the risk of infection for a given population is considerably more useful than its filtration efficiency (FE). The effect of the mask on the infection profile is complicated to estimate as it depends strongly upon the behavior of the affected population. A recently introduced tool known as the dynamic-spread model is well suited for performing population-specific risk assessment. The dynamic-spread model was used to simulate the performance of a variety of mask designs (all used for source control only) in different COVID-19 scenarios. The efficacy of different masks was found to be highly scenario dependent. Switching from a cotton T-shirt of 8% FE to a 3-layer cotton-gauze-cotton mask of 44% FE resulted in a decrease in number of new infections of about 30% in the New York State scenario and 60% in the Harris County, Texas scenario. The results are valuable to policy makers for quantifying the impact upon the infection rate for different intervention strategies, e.g., investing resources to provide the community with higher-filtration masks.

**Keywords:** COVID-19; SIR model; infection-spread model; facemask; dynamic-spread model

## 1. Introduction

To limit the spread of COVID-19 during times when respirators are not widely available, extensive use has been made of homemade masks [1,2]. A number of groups [1,3–7] measured the

filtration-efficiency (FE) of homemade masks against simulated COVID-19 particles. Drewnick et al. [1] examined a wide variety of materials used in homemade face masks. Guha et al. [3] considered different modes of transmission including fomites. Maher et al. [8] measured the ability of different homemade masks to filter aerosol droplets and correlated the results with fluid velocity fields in the vicinity of the mask. While FE is a useful measure of the integrity of the barrier design, a more important measure for public-health officials and policy makers designing intervention strategies is the effect of the barrier on the infection rate for the population of interest.

One way to translate FE values into rates of infection spread is using computational models such as susceptible-infected-removed (SIR) models [9–15]. The models attempt to incorporate the factors most strongly affecting the infection dynamics for the scenario of interest. Mask-use compliance and vaccination rates [16–18] for the population under consideration constitute important behavioral factors. Environmental conditions such as pollution levels, wind characteristics and humidity that prevail in the infection scenario also affect the infection dynamics [19–21]. An SIR-type model that is particularly well adapted to incorporating characteristics of a specific scenario into infection-rate predictions is the dynamic-spread model [16,22]. Effects such as mask compliance (as a function of time) and level of social distancing are automatically introduced through the calibration of the dynamic-spread function using published infection curves. Environmental factors specific to the scenario of interest are also indirectly incorporated into the calibration process. The dynamic-spread model was recently employed by D'Souza et al. [16] to highlight the different changes in infection dynamics for different locations when the same intervention strategy is considered.

In this paper, we employ the dynamic-spread model to compare a variety of mask designs in terms of the change in infection rates they produce in different COVID-19 scenarios. The scenarios are those considered in [16] the first wave of COVID-19 in New York City, the first wave of COVID-19 in New York State, the spread of COVID-19 aboard the Diamond Princess Cruise ship in 2020 and the transmission of COVID-19 after Memorial Day 2020 in Harris County, Texas. A baseline scenario is first established by calibrating the dynamic-spread function using published infection curves for COVID-19 for each scenario. A homemade 3-layer mask is assumed for the baseline scenario. The model then estimates the change in the infection rate when intervention strategies involving alternative masks are considered.

From a public health perspective, the goal of the simulations involving the four infection scenarios is to present a general-purpose tool that can be used in any scenario where reliable infection data is available to assess how different mask designs affect the risk of infection for that specific scenario. As a specific example, it is known [1] that the filtration efficiency of a surgical mask is about 8 times as high as the filtration efficiency of a mask made from a cotton t-shirt. To a policy maker deliberating whether to invest resources into procuring surgical masks and persuading the population to use them, the tradeoff in terms of reduction in risk purchased with the resources is valuable information. A factor of 3 or 4 reduction in risk may be acceptable to the official but a factor of 1.5 may persuade the official to use the resources some other way. Common mask designs are featured in the simulations and hence the results of the computations are of public health relevance. More importantly however, the simulations illustrate how the dynamic-spread tool can compare intervention strategies involving any laboratory-tested masks on the basis of infection risk for a general infection scenario of interest.

## 2. Methods

We first present an overview of the model and subsequently provide the mathematical description.

### *2.1. Proposed model*

The dynamic-spread approach is based upon an SIR model that was extended to additionally simulate the droplet distribution. The model was developed by Stilianakis and Drossinos [23] and modified by Myers et al. [24] to account for the presence of synthetic barriers to virus transmission. In [22] the model was further adapted to allow the droplet production rate and disease transmission rate to vary with time. Allowing these quantities to vary continuously with time enabled the model to simulate population behavior in a systematic way. In the mathematical development several clusters of parameters emerge, one of which is a continuous function of time. The time-dependent parameter is the dynamic-spread function. The dynamic-spread function itself satisfies a differential equation with variable coefficients. The coefficient functions derive from the published infection profiles (e.g., number of new infections per day) for the scenario of interest. Once the coefficient functions are provided, the model is calibrated by solving the differential equation. Thus, the dynamic-spread function is calibrated in a continuous fashion using real-world data. This approach is analogous to the manner in which artificial-intelligence systems are calibrated except that only a single data set is required. This procedure is very different from the calibration process for most SIR models where calibration consists of prescribing representative values for the many parameters appearing in the equations. When the important factors affecting the infection dynamics change (e.g., social distancing is instituted), parameter estimation re-occurs at these discrete times with the conventional SIR models.

Once calibrated, the dynamic-spread model can then be used to predict the course of the epidemic that would have occurred for different intervention strategies than those originally used in the scenario. In the current study, the different intervention strategies take the form of different mask designs. We emphasize that because the dynamic-spread model requires calibration using infection data already available for all time points of interest it is not a forecasting model. Rather, it is a comparison model. However, the results of the model can be valuable for designing countermeasures to future waves of epidemics.

### *2.2. Parameter values*

As just noted, the most important parameter of the model is the dynamic-spread function, which is completely specified from the temporal infection profile for the scenario of interest. Factors affecting the infection dynamics such as population behavior or environmental influences are indirectly incorporated in the coefficient functions as these factors determine the coefficient functions and ultimately the dynamic-spread function. However, these factors are never explicitly parameterized.

Two parameters do need to be prescribed in the dynamic-spread approach. They are the droplet removal rate and the infection recovery rate. As shown in [22], the droplet removal rate can be determined from the reproduction number $R_0$. For a given epidemic, there exists a range of published estimates for the infection recovery rate and the reproduction number. We sample the range of the two parameters using a Monte Carlo approach and we perform simulations for all of the sampled values. The corresponding distribution of outputs from the model is used to ascribe an uncertainty to our

estimates. Details of the uncertainty analysis can be found in [16].

### *2.3. Mathematical description*

The intermediate steps in the derivation of the dynamic-spread model are provided in [22]. Here, we present the final form of the equations governing the evolution of the number of new infections per day *U(t)* and the total number of infected persons *I(t)*:

$$\frac{dU}{dt} = \delta I - \lambda U + \frac{U}{\delta}\frac{d\delta}{dt} \tag{1a}$$

$$\frac{dI}{dt} = U - \gamma I \tag{1b}$$

All the variables in the equations are rendered dimensionless using the transformations discussed in [22]. Time is normalized by the temporal window of interest Δwhich we often take to be the time from the first lockdown order to the first maximum in the recorded number of new infections per day. $\lambda = \Delta/n$ is the dimensionless droplet removal rate and $\gamma = \Delta\mu_I$ is the dimensionless infection recovery rate, $\mu_I$ being the dimensional infection recovery rate. The function *d(t)* is the dynamic spread function defined by

$$\delta(t) = \tilde{\beta}(t)\kappa(t)\Delta^2 \tag{1c}$$

where $\tilde{\beta}$ is the transmission rate and $\kappa$ is the droplet production rate, both of which are assumed to vary with time. The dynamic spread function also satisfies a differential equation with variable coefficients. The equation for the baseline scenario is

$$\frac{d\delta_b}{dt} = -\frac{I_b}{U_b}\delta_b^2 + \left(\lambda + \frac{1}{U_b}\frac{dU_b}{dt}\right)\delta_b \tag{2}$$

where the "b" subscript denotes baseline. When the baseline dynamic spread function obtained from Eq (2) is inserted back into the governing Eq (1a),(1b), the baseline populations $U_b(t)$ and $I_b(t)$ are reproduced within numerical tolerances. The dynamic-spread approach is initiated when the spread function is modified to simulate an alternative intervention strategy to an existing scenario and Eq (1) are used to estimate the modified infection rates for the scenario under the hypothesized intervention. It was shown in [22] that the modified spread function appropriate for analyzing a change in outward barrier filtration efficiency ($FE_{out}$) from the baseline value $FE_{out,b}$ to the modified value $FE_{out,mod}$ is

$$\delta_{mod}(t) = \frac{\left[1-\frac{FE_{out,mod}}{FE_{out,b}}(1-[\delta_b(t)/\delta(0)]^{\epsilon_\kappa})\right]}{[\delta_b(t)/\delta(0)]^{\epsilon_\kappa}}\delta_b(t) \tag{3}$$

Here, $\epsilon_\kappa$ is the fraction of the change in *d(t)* due to changes in droplet production. As discussed in [16,22], we choose $\epsilon_\kappa = 1/5$.

- Estimation of mask compliance

In predicting the effect of mask usage by a population in a given scenario, knowledge of the fraction of the population using the mask is valuable. The variation in this compliance fraction over

time is also important information. The dynamic-spread approach can compute the mask compliance throughout the window for which the baseline infection curves are available. In terms of the dynamic-spread function, the mask compliance is given by [22].

$$f_i(t) = \frac{1-[\delta(t)/\delta(0)]^{\epsilon\kappa}}{FE_{out}} \tag{4}$$

The function *d(t)* is specific to the scenario under consideration and will vary across scenarios, manifesting the different population behaviors in the different locations. The derived compliance profile consequently also varies across scenarios.

### *2.4. Mask types considered*

Nine different mask types and one case without any barrier were considered in the simulations. The mask labels and filtration efficiencies were taken from Drewnick et al. [1]. Filtration efficiencies were averaged over 2 size ranges 30 nm to 250 nm and 500 nm to 10 microns. As described in the next section, both ranges are considered in the calculations. The penetration values equal to 1–FE for the masks are provided in Table 1. Additional features of the masks may be found in [1].

**Table 1.** Mask materials and penetration values for barriers considered in the simulations.

| Characteristics of masks involved in simulations | | | |
|---|---|---|---|
| Mask Label | Material | Penetration 30 nm to 250 nm (%) | Penetration 500 nm to 10 microns (%) |
| Surgical self-made mask | 100% cotton (2 outer layers), 100% synthetic fiber gauze (4 inner layers) | 56 | 24 |
| Vacuum cleaner bag | Unspecified synthetic material | 5 | 1 |
| Encasement 1 | 70% polyester, 30% polyamide | 28 | 4 |
| Surgical mask | Multi-layer non woven material | 38 | 9 |
| Encasement 2 | 100% polypropylene | 49 | 10 |
| Poplin | 100% cotton | 60 | 19 |
| Microfiber terry | 100% microfiber | 69 | 40 |
| Muslin | 100% cotton | 80 | 65 |
| Cotton shirt fabric | 100% cotton | 92 | 55 |
| No mask | --- | 100 | 100 |

### *2.5. Scenarios considered*

Four COVID-19 infection scenarios were chosen for examining the influence of the different mask designs on the infection rate. The four scenarios, previously introduced in [16], were originally chosen because they were high profile during COVID-19 and they provided a variety in terms of factors affecting infection dynamics, including total population and population density, attitudes toward masking, weather and initiation time (after beginning of epidemic) for the study. The locations for the four scenarios are New York City, New York State, Diamond Princess cruise ship and Harris County, Texas. For New York City, New York State and the Diamond Princess cruise ship, the scenario

began at the first lockdown order and finished at the time of the first maximum in the profile of new infections per day. For Harris County, the scenario of interest begins on May 31, 2020, roughly the beginning of the surge in cases after Memorial Day in 2020 and completes at the first large peak in new infections (averaging over 7 days) after Memorial Day. The total duration was 15 days for New York State, 20 days for New York City, 12 days aboard the Diamond Princess and 26 days in Harris County, Texas. Further details of all the scenarios may be found in [16].

### *2.6. Data analysis*

In the computations, the surgical self-made mask from Table 1 was chosen as baseline. The penetration of the other masks relative to baseline was defined by:

$$P_r = \frac{P_{mask} - P_{baseline}}{P_{baseline}}, \tag{5}$$

where $P_r$ is the relative penetration, and $P_{mask}$ and $P_{baseline}$ are the penetrations (from Table 1) for the mask of interest and the baseline mask. As an example, the Encasement 1 mask in Table 1 has a relative penetration of -50 % in the 30 nm to 250 nm particle size bin. The rate of infection for the mask of interest relative to the infection rate for the baseline mask was quantified by a relative number of new infections at the end of the time interval:

$$U_r = \frac{U_{mask}(t_{final}) - U_{baseline}(t_{final})}{U_{baseline}(t_{final})}. \tag{6}$$

Here $U_{mask}(t_{final})$ is the number of new infections at the end of the time interval, obtained from the solution of Eqs (1)–(3), for the mask of interest. $U_{baseline}(t_{final})$ is the number of new infections at the end of the time interval for the baseline mask. Relative numbers of new infections were calculated for both droplet size bins and each of the four scenarios.

An additional metric used to compare the mask designs is the relative likelihood of infection, $L_r$. This quantity is obtained by summing the number of new infections per day over the total simulation period for the mask of interest and dividing by the same sum for the case of no mask. Calculations are performed for both size bins and all four scenarios. Since the normalizing quantity is the number of infections for no mask, $L_r$ is a measure of the benefit of wearing a mask in the scenario of interest.

For calculations involving a given size bin, the appropriate outward filtration efficiency from Table 1 was used in Eq (3). This procedure assumes that the infection spread was dominated by airborne droplets of the given size. It also assumes that only source-control is modeled; susceptible persons are not protected from incoming droplets.

## 3. Results

The relative number of new infections for the 4 scenarios along with the relative penetration for the masks are shown in Figure 1 for the lower droplet size bin (30 nm to 250 nm).

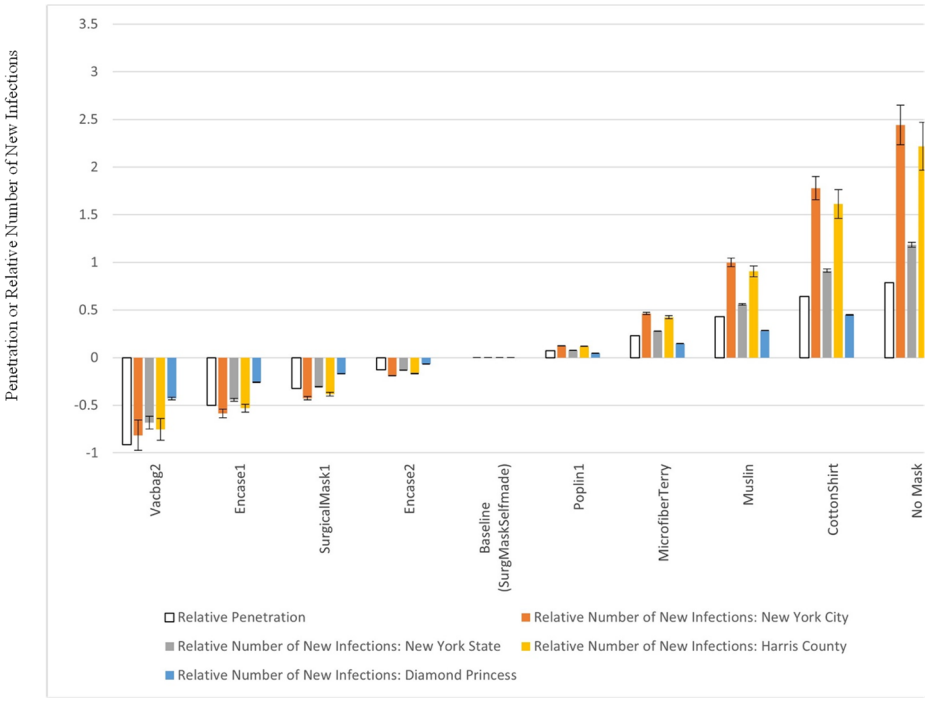


a. Droplet size bin is 30 nm to 250 nm. Labels along horizontal axis correspond to the names of the mask materials in Table 1.

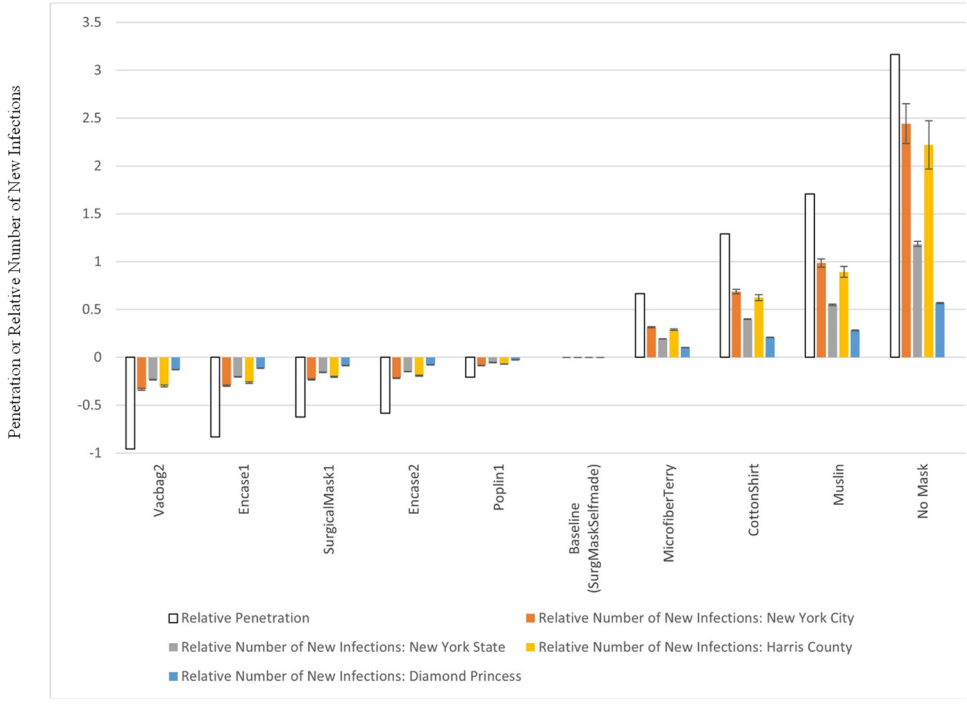


b. Droplet size bin is 500 nm to 10 microns. Labels along horizontal axis correspond to the names of the mask materials in Table 1.

**Figure 1.** Relative number of new infections per day (along with relative penetration) for the different mask designs, in the 4 different scenarios.

The first bar in each group (uncolored) is the relative penetration for the mask and the other 4 bars represent the relative number of new infections per day for the 4 scenarios. Since the surgical self-made mask is the baseline, its relative penetration and relative number of new infections are zero. Groups to the right of baseline represent masks with higher penetration (lower filtration efficiency) and consequently higher infection rates. Groups to the left have lower penetration and lower infection rates. For the cotton t-shirt, the penetration is 60% higher than baseline and the numbers of new infections per day range from 40% larger than baseline (on the Diamond Princess cruise liner) to 180% above baseline (in New York City). For the vacuum bag, the penetration is about 90% less than baseline and the numbers of new infections range from 40% (Diamond Princess) to 80% (New York City) less than baseline.

The corresponding results for the larger droplet-size bin (500 nm to 10 microns) are shown in Figure 1b.

In contrast to the smaller size bin, for the larger droplets the relative penetration exceeds (in magnitude) the relative number of new infections in all cases. For example, for the cotton t-shirt the relative penetration is 130% more than baseline but the relative number of new infections varies between about 20% (Diamond Princess) to 70% (New York City) higher than baseline. For the vacuum bag, the relative penetration is over 90% less than baseline while the numbers of new infections range from about 10% (Diamond Princess) to 30% (New York City) less than baseline.

The relative likelihood of infection is shown in Figure 2a (Diamond Princess), Figure 2b (New York City), Figure 2c (New York State), and Figure 2d (Harris County).

To aid in interpretation we consider the muslin mask and the New York State scenario (Figure 2c). For both size bins, the likelihood of an individual becoming infected when infected persons use the mask is 80% of the likelihood when no source protection is used. The relative likelihood of infection spans the range from about 90% (Cotton T-shirt, Diamond Princess scenario) to 20% (vacuum bag, Harris County scenario). The variation in relative likelihood of infection across mask types is weak (less than a factor of two variation) for the Diamond Princess, strong (factor of 4 or 5) for Harris County and New York City and intermediate (factor of 2.5) for New York State. The variation between droplet size bins is not strong, less than 10% when averaged across all mask types and scenarios.

A public health situation in which the results of Figure 2a–d could be useful is the following. We suppose a policy maker in Harris County, TX wanted to avoid the surge in COVID-19 infections during a subsequent re-opening and the official knew that the majority of the infected population was either not using masks or using masks made from cotton shirts (the right side of Figure 2d). The official could entice the population to switch to surgical masks by procuring these masks and informing the public that the infection rate for the county could have been less than half of what it was during the previous re-opening if the surgical masks had been deployed. For added incentive, other models could be used to convert infections to hospitalizations.

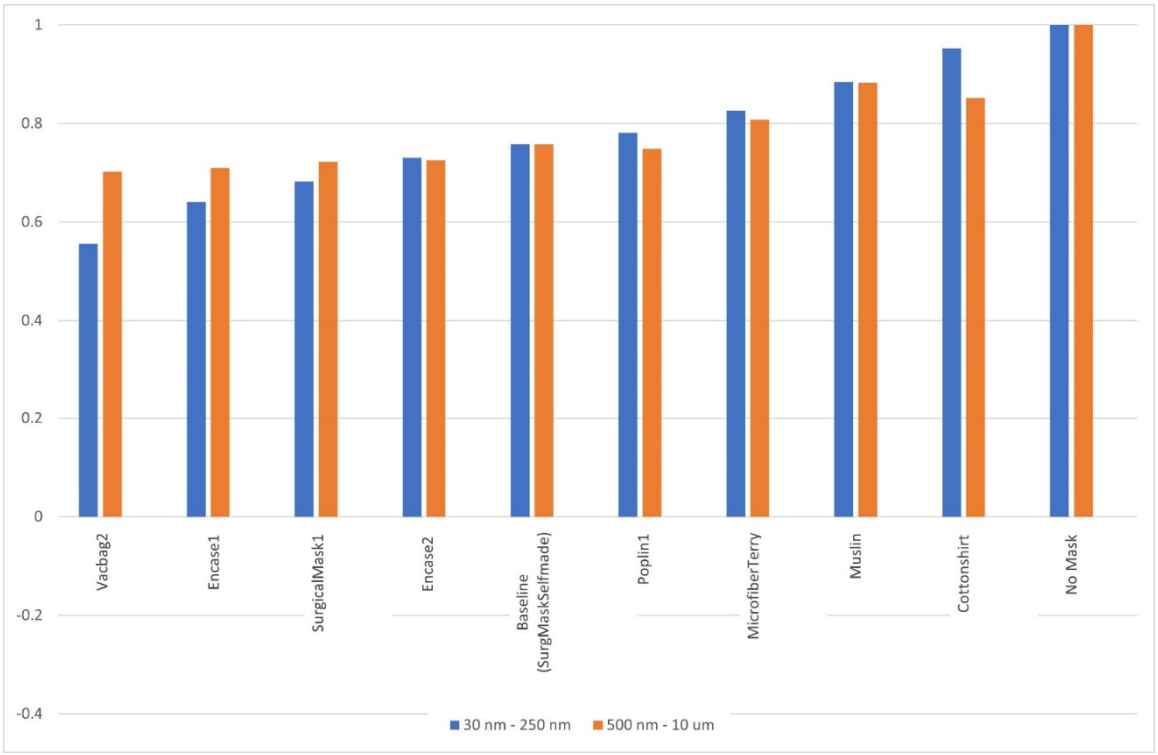


a. Diamond Princess scenario.

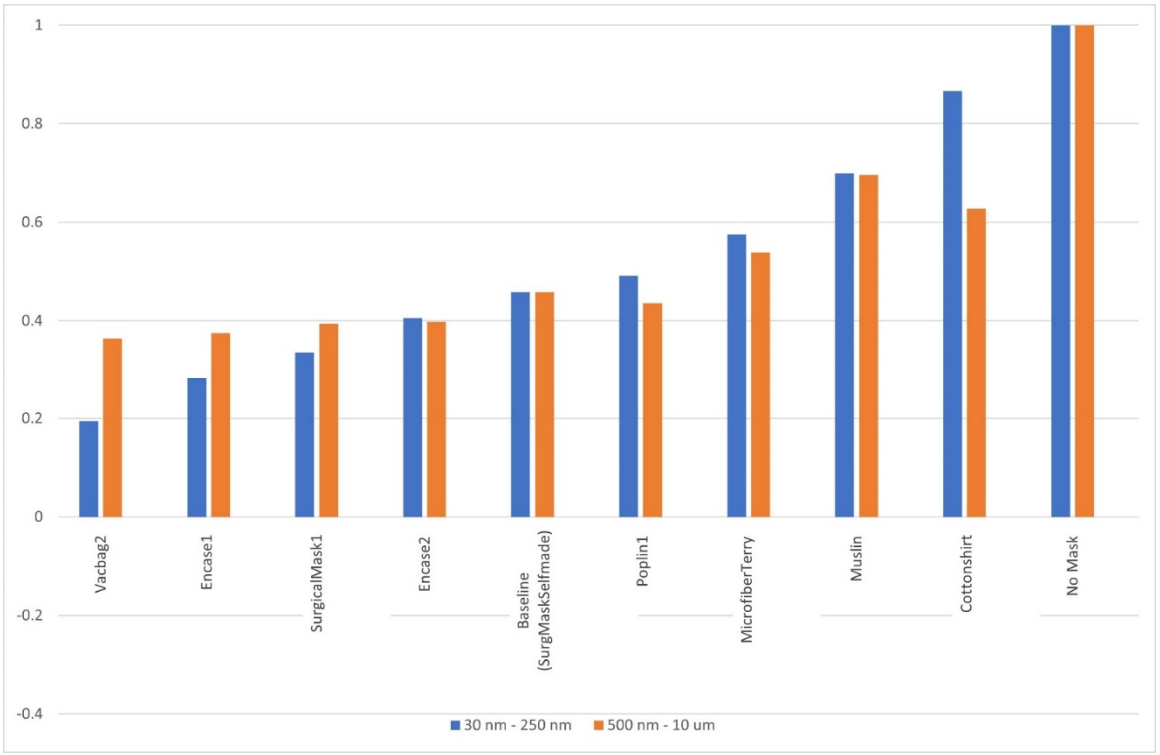


b. New York City scenario.

*Continued on next page*

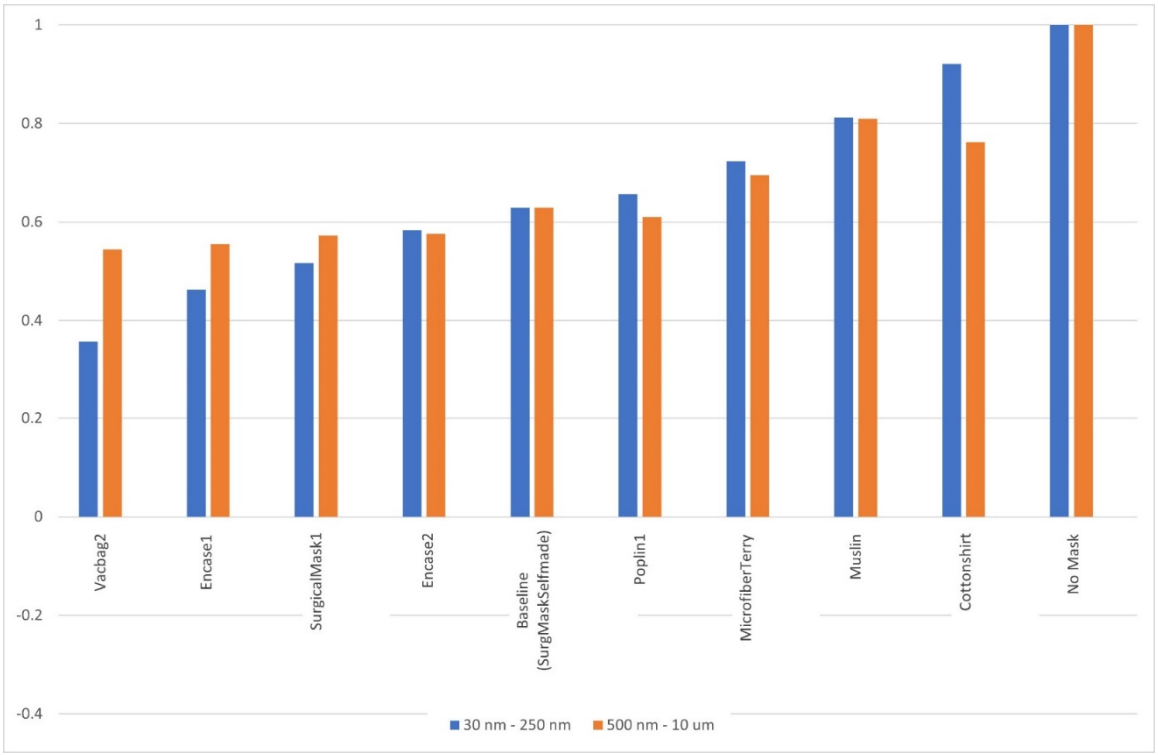


c. New York State scenario.

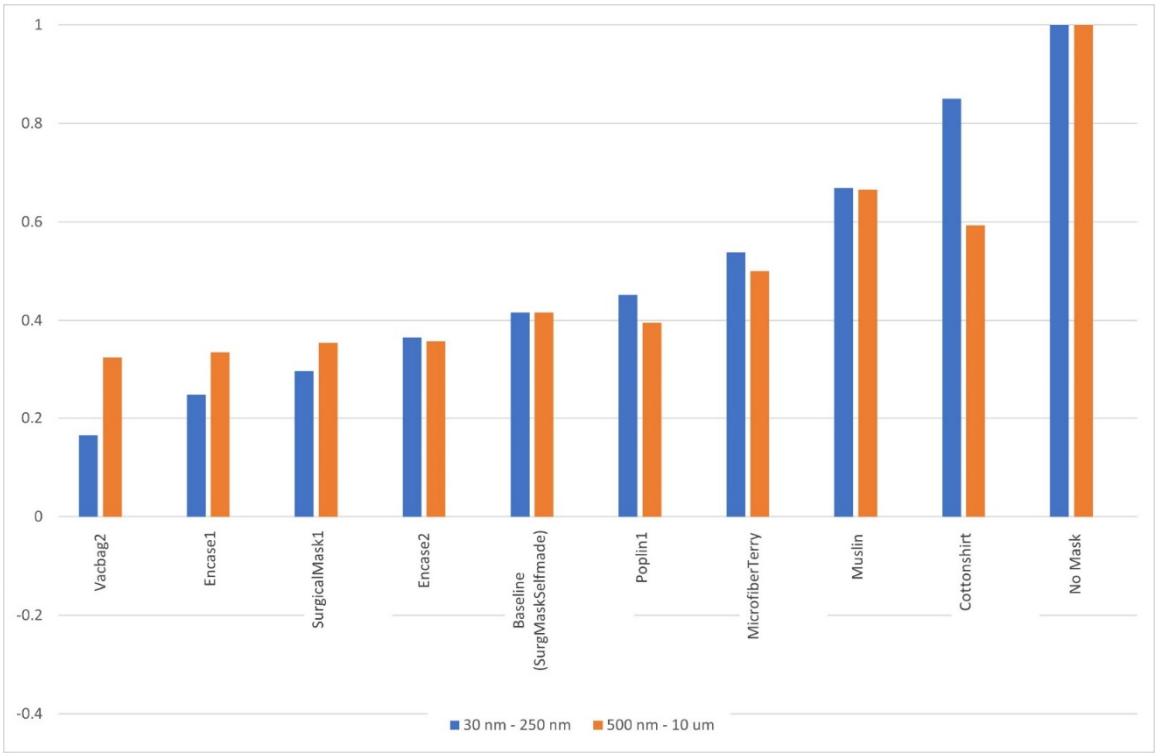


d. Harris County scenario.

**Figure 2.** Relative likelihood of infection over the entire time interval for both droplet size bins.

## 4. Discussion

Given the unconventional nature of the dynamic-spread model relative to other SIR models, it is important to elucidate the capabilities and limitations of the model. An advantage of the dynamic-spread model is that it does not require prescription of parameters. (Other than the infection rate and the reproduction number, for which a range of values is selected from published values and used to create an uncertainty estimate.) By calibrating the model using data sets from actual infection scenarios (via the baseline functions $I_b(t)$ and $U_b(t)$ in Eq (2)), factors such as weather conditions, social-distancing tendencies, vaccination rates and attitudes toward mask deployment are automatically incorporated into the analysis. For example, calibration using infection data from the Delta variant of COVID-19 would yield a different dynamic-spread function than using data from the Omicron variant, even for the same population. Then, the model might predict that switching from a cotton cloth mask to a surgical mask would yield different reductions in risk for the Omicron variant than the Delta variant. A disadvantage of not parameterizing the different factors explicitly is that the effects of the different factors cannot be readily studied. For instance, it is shown in [23] that the transmission rate where $\tilde{\beta}$ which is part of the dynamic spread function (See Eq (1c)) is dependent upon the atmospheric conditions including wind speed. Since the dependence is not modeled, the sensitivity of the model results to atmospheric conditions cannot be studied in a systematic manner.

Another limitation of the model is that the droplet size bin most responsible for the infections is not known. The information (e.g., droplet spread due to wind speed) implicitly contained in the dynamic-spread function may pertain to one size in actuality while the calculations were performed for another. The droplet sizes most strongly influencing the spread of infection may depend upon the weather conditions for the given scenario. Further research is necessary to address the issue of most influential droplet size on the spread of COVID-19.

The calculated infection rate responded to changes in mask type differently for the two droplet size bins. For the smaller droplets, a decrease in penetration (increase in FE) relative to baseline produced a comparable decrease in numbers of new infections (left half of Figure 1a). However, an increase in penetration (decrease in FE) produced relative increases in numbers of new infections that are typically much higher (right half of Figure 1a). This situation illustrates that mask permeability measures (FE or penetration) may not be good quantitative indicators of infection risk.

For the larger droplets (Figure 1b), a change in penetration (relative to the baseline mask) of a given amount produced a change in the number of new infections that was considerably smaller. Interestingly, this trend was true for both increases and decreases in mask penetration. The lower response of the infection rate to a change in mask design, for the larger droplets relative to that for the smaller droplets, is due in large part to the lower mask compliance (Eq (4)) for the baseline mask, for the higher FE values associated with the larger droplets. The compliance for the baseline mask at the end of the simulation interval is shown in the table below. Computed compliances for the larger particle size ranges from about 17% to 36%, while for the smaller particles the compliance is between about 29% to 62%. We note that the compliance at the initial time is zero, illustrating the gradual adoption of the mask by the given population. The role of the compliance is discussed further in [16].

The influence that a given mask design has over the infection profile is highly dependent upon the infection scenario. The differences between scenarios and the effect of the differences upon the infection rate were discussed in [16]. Here we highlight a few dominant effects. The relatively weak dependence of the number of new infections upon mask design exhibited in the Diamond Princess

scenario (e.g., Figure 2a) is due in large part to the relatively low compliance (Eq (4)) compared to the other scenarios. In New York City, the infection rate was high initially, and the mask compliance increased relatively quickly. The result was a large value of the spread function (Eq (2)) and its derivative, providing an opportunity for different mask designs to have a substantial impact. In Harris County, the derivative of the spread function was positive (consistent with the rapid rise in new infections following Memorial Day), making the number of new infections sensitive to increases in the mask penetration (e.g., right half of Figure 1). The sensitivity of infection dynamics to a specific scenario is an important feature for which the spread function can provide considerable insight but simple measures of mask integrity (e.g., FE alone) cannot.

Figure 1 provides the change in infection rate (associated with a change in mask design relative to baseline) in terms of the numbers of new infections at the end of the time interval. As the end of the time interval was defined in terms of the maximum number of new infections of COVID-19 per day (except for Harris County), the infection metric was necessarily worst case, at least for the first wave of COVID-19. The number of new infections integrated over the entire period, plotted in Figure 2, is a less severe measure of infection, since the initial number of new infections was low. Hence, the effect of increasing the filtration efficiency is less dramatic than in Figure 1. Additionally, the variation across scenarios for a given mask was not as strong when the risk is integrated over the entire time duration and normalized by the no-mask case compared with the risk at the end of the time window. This is particularly true of the higher-risk masks. Still, the following conclusion can be drawn regarding the risk integrated over the entire time window studied and derived from the four scenarios considered: when the infected population deploys a mask, the calculated likelihood of infection is reduced between 30% to 70% relative to infected persons not using a mask at all.

The investigation by Schmitt and Wang [25] enables a meaningful comparison with the present study. Using an SIR-type model, Schmitt and Wang computed the probability of infection for three types of masks the filtering face pieces (FFP's), surgical masks and cloth masks. The mask penetration values, derived from Table 2 of Schmitt and Wang assuming the highest leakage rates, were 0.43 (FFP), 0.56 (surgical masks), and 0.93 (cloth). The corresponding probabilities of infection when the barriers are used as source control are $1.7 \times 10^{-7}$ (FFP), $2.3 \times 10^{-7}$ (surgical mask) and $3.8 \times 10^{-7}$ (cloth). The probability of infection for a given mask design relative to that for the surgical mask was 0.72 for the FFP and 1.7 for the cloth mask. That is, an individual is 1.7 times as likely to be infected when cloth masks are deployed by the infected population than when the infected population deploys surgical masks. The triplet of masks from the present study most closely matching those of Schmitt and Wang in penetration are the surgical mask, Poplin and cotton T-shirt. The penetration values are 0.38 (Table 1, smaller size droplets) for the surgical mask, 0.60 for Poplin, and 0.92 for the T-shirt. From Figure 2a–d, the probability of infection for the surgical mask divided by the probability of infection for the Poplin mask is 0.86 +/- 0.9 for the Diamond Princess scenario, 0.69 +/- 0.7 for New York City, 0.79 +/- 0.8 for New York State, and 0.79 +/- 0.8 for Harris County. As noted above, the corresponding relative probability for the study by Schmitt and Wang is 0.72. The probabilities of infection for the T-shirt divided by those for the Poplin mask are: 1.2 +/- 0.1 for the Diamond Princess, 1.8 +/- 0.2 for New York City, 1.4 +/- 0.1 for New York State and 1.9 +/- 0.2 for Harris County. For comparison, the relative probability computed by Schmitt and Wang for the similar masks is 1.7. We conclude the following: 1) the performance (in reducing infection rate) of a given type of mask, relative to the performance of a baseline mask type, agrees well between the investigation by Schmitt and Wang and the present study and 2) the performance of the masks predicted by Schmitt and

Wang matches that of our New York City scenario quite closely.

**Table 2.** Compliance values for the baseline mask, at the end of the time window for both size bins.

| Compliance values for baseline mask | | |
|---|---|---|
| | 250 nm–500 nm | 500 nm–10 um |
| NY City | 0.5198 | 0.3009 |
| NY State | 0.6190 | 0.3584 |
| HC | 0.2665 | 0.1543 |
| DP | 0.2890 | 0.1673 |

The results in Figure 1 were normalized relative to the 3-layer "self-made surgical mask". For direct comparison of two masks (say masks 1 and 2) other than the self-made surgical mask, the relative number of new infections in Eq (6) can be rewritten as $U_1/U_{baseline}–1$ and $U_2/U_{baseline}–1$. Adding 1 to each of these quantities and dividing one result by the other gives $U_1/U_2$ (or $U_2/U_1$) at the end of the time interval for the given scenario.

We emphasize that masks were used only for source control in our study, i.e., they only affected the virus transmitted by infected persons. Incorporation of masks worn by non-infected persons for protection is an important future direction of the model. This extension requires the inward filtration efficiency for the masks of interest, as well as a prescription of the gap profile between the face and the barrier. For the present, we note that the calculated reductions in infection likelihood enabled by masks are an underestimate.

The number of mask designs emerging during the COVID-19 was too large for the present study to be comprehensive. In particular, designs involving multiple layers were not covered thoroughly in our study. One of the important goals of the study was to raise awareness of the drawbacks of using filtration efficiency alone for making decisions regarding infection countermeasures. Interested users can implement the tool defined in Eqs (1)–(4) to estimate the impact of their particular mask on the infection dynamics for the scenario of interest. The model is simple and can be readily used by persons not familiar with the governing equations or parameters characterizing the mechanisms of infection spread. A user-friendly version of the tool incorporating the 4 scenarios featured in this article will be released by the authors in the near future.

## 5. Conclusions

The dynamic-spread model was used to convert the mechanical property of mask filtration efficiency to infection risk which is more important for public-health decision making. A variety of mask designs were considered. It was shown that the utility, in terms of risk reduction, of increasing the filtration efficiency of a mask is highly scenario dependent. For example, switching from a cotton T-shirt of 8% FE to a 3-layer (cotton-gauze-cotton) mask of 44% FE resulted in a decrease in number of new infections of about 30% in the New York State scenario and 60% in the Harris County, Texas scenario. The dynamic-spread model involves no parameter estimation and is simple to use making it a useful component in the toolbox of policy makers designing strategies to counter epidemics.

## Use of AI tools declaration

The authors declare they have not used Artificial Intelligence (AI) tools in the creation of this article.

## Acknowledgments

This work was funded internally by the U. S. Food and Drug Administration.

## Conflict of interest

The authors declare there is no conflict of interest.

## References

1. F. Drewnick, J. Pikmann, F. Fachinger, L. Lasse Moormann, F. Sprang, S. Borrmann, Aerosol filtration efficiency of household materials for homemade face masks: Influence of material properties, particle size, particle electrical charge, face velocity, and leaks, *Aerosol Sci. Technol.*, **55** (2021), 63–79. https://doi.org/10.1080/02786826.2020.1817846
2. K. H. Y. Hahn, G. Bhaduri, Mask up: Exploring cross-cultural influences on mask-making behavior during the COVID-19 pandemic, *Clothing Text. Res. J.*, **39** (2021), 297–313. https://doi.org/10.1177/0887302X211012747
3. S. Guha, A. Herman, I. A. Carr, D. Porter, R. Natu, S. Berman, et al., Comprehensive characterization of protective face coverings made from household fabrics, *PLoS One*, **16** (2021), e0244626. https://doi.org/10.1371/journal.pone.0244626
4. National Academies of Sciences, Engineering, and Medicine 2020, Rapid expert consultation on the effectiveness of fabric masks for the COVID-19 Pandemic, in *Rapid Expert Consultations on the COVID-19 Pandemic*, The National Academies Press, 2020. https://doi.org/10.17226/25776
5. J. Howard, A. Huang, Z. Li, Z. Tufekci, V. Zdimal, H. M. van der Westhuizen, et al., An evidence review of face masks against COVID-19, *Proc. Nat. Acad. Sci.*, **118** (2021), e2014564118. https://doi.org/10.1073/pnas.2014564118
6. C. Varallyay, N. Li, B. Case, B. Wolf, Material suitability testing for nonmedical grade community face masks to decrease viral transmission during a pandemic, *Disaster Med. Public Health Prep.*, **15** (2021), e26–e32. https://doi.org/10.1017%2Fdmp.2020.262
7. B. Osman, H. Mahmud, N. L. A. Rani, T. A. Ibrahim, I. Ismail, Household materials for homemade masks: how effective are they, *Malays. J. Med. Health Sci.*, **17** (2021), 59–64.
8. B. Maher, R. Chavez, G. C. Q. Tomaz, T. Nguyen, Y. Hassan, A fluid mechanics explanation of the effectiveness of common materials for respiratory masks, *Int. J. Infect. Dis.*, **99** (2020), 505–513. https://doi.org/10.1016/j.ijid.2020.07.066
9. R. O. J. H. Stutt, R. Retkute, M. Bradley, C. A. Gilligan, J. Colvin, A modelling framework to assess the likely effectiveness of facemasks in combination with 'lock-down' in managing the COVID-19 pandemic, *Proc. Royal Soc.*, **476** (2020), 20200376. https://doi.org/10.1098/rspa.2020.0376

10. G. Giordano, F. Blanchini, R. Bruno, P. Colaneri, A. Di Filippo, A. Di Matteo, et al., Modelling the COVID-19 epidemic and implementation of population-wide interventions in Italy, *Nat. Med.*, **26** (2020), 855–860. https://doi.org/10.1038/s41591-020-0883-7
11. I. Cooper, A. Mondal, C. G. Antonopoulos, A SIR model assumption for the spread of COVID-19 in different communities, *Chaos, Solitons Fractals*, **139** (2020), 110057. https://doi.org/10.1016/j.chaos.2020.110057
12. A. L. Bertozzi, E. Franco, G. Mohler, M. B. Short, D. Sledge, The challenges of modeling and forecasting the spread of COVID-19, *Proc. Nat. Acad. Sci.*, **117** (2020), 16732–16738. https://doi.org/10.1073/pnas.2006520117
13. C. N. Ngonghala, E. Iboi, S. Eikenberry, M. Scotch, C. R. MacIntyre, M. H. Bonds, et al., Mathematical assessment of the impact of non-pharmaceutical interventions on curtailing the 2019 novel Coronavirus, *Math. Biosci*., **325** (2020), 108364. https://doi.org/10.1016/j.mbs.2020.108364
14. S. E. Eikenberry, M. Mancuso, E. Iboi, T. Phan, K. Eikenberry, Y. Kuang, et al., To mask or not to mask: modeling the potential for face mask use by the general public to curtail the COVID-19 pandemic, *Infect. Dis. Modell.*, **5 (**2020), 293–308. https://doi.org/10.1016/j.idm.2020.04.001
15. J. Fernández-Villaverde, C. I. Jones, Estimating and simulating a SIRD Model of COVID-19 for many countries, states, and cities, *J. Econ. Dyn. Control*, **140** (2022), 104318. https://doi.org/10.3386/w27128
16. G. D'Souza, J. Osborn, S. Berman, M. Myers, Comparison of effectiveness of enhanced infection countermeasures in different scenarios, using a dynamic-spread-function model, *Math. Biosci. Eng.*, **19** (2022), 9571–9589. https://doi.org/10.3934/mbe.2022445
17. C. Deschanvres, T. Haudebourg, N. Peiffer-Smadja, K. Blanckaert, D. Boutoille, J. C. Lucet, et al., How do the general population behave with facemasks to prevent COVID-19 in the community? A multi-site observational study, *Antimicrob. Resist. Infect. Control*, **10** (2021), 1–6. https://doi.org/10.1186/s13756-021-00927-6.
18. K. Abid, H. Ahmed, Y. A. Bari, M. Younus, Z. P. Khambati, A. Imran, et al., Perceived barriers to facemask adherence in the COVID-19 pandemic in Pakistan-A cross-sectional survey, *PLoS One*, **17** (2022), e0267376. https://doi.org/10.1371%2Fjournal.pone.0267376
19. M. Coccia, Sources, diffusion and prediction in COVID-19 pandemic: lessons learned to face next health emergency, *AIMS Public Health*, **10** (2023), 145–168. https://doi.org/10.3934/publichealth.2023012
20. A. Núñez-Delgado, E. Bontempi, M. Coccia, M. Kumar, J. L. Domingo, SARS-CoV-2 and other pathogenic microorganisms in the environment, *Environ. Res.*, **201** (2021), 111606. https://doi.org/10.1016/j.envres.2021.111606
21. M. Coccia, Pandemic prevention: Lessons from COVID-19, *Encyclopedia*, **1** (2021), 433–444. https://Doi.org/10.3390/encyclopedia1020036
22. J. Osborn, S. Berman, S. Bender-Bier, G. D'Souza, M. Myers, Retrospective analysis of interventions to epidemics using dynamic simulation of population behavior, *Math. Biosci.*, **341** (2021), 108712. https://doi.org/10.1016/j.mbs.2021.108712
23. N. I. Stilianakis, Y. Drossinos, Dynamics of infectious disease transmission by inhalable respiratory droplets, *J. R. Soc. Interface*, **7** (2010), 1355–1366. https://doi.org/10.1098/rsif.2010.0026

24. M. Myers, P. Hariharan, S. Guha, J. Yan, A mathematical model for assessing the effectiveness of protective devices in reducing risk of infection by inhalable droplets, *Math. Med. Biol.*, **35** (2018), 1–23. https://doi.org/10.1093/imammb/dqw018
25. J. Schmitt, J. Wang, A critical review on the role of leakages in the facemask protection against SARS-CoV-2 infection with consideration of vaccination and virus variants, *Indoor Air*, **32** (2022), e13127. https://doi.org/10.1111/ina.13127


AIMS Press